

Giant resistance switching in metal-insulator-manganite junctions: Evidence for Mott transition

Rickard Fors,* Sergey I. Khartsev, and Alexander M. Grishin

Condensed Matter Physics, Royal Institute of Technology, Electrum 229, SE-164 40 Stockholm-Kista, Sweden

(Received 9 June 2004; revised manuscript received 30 September 2004; published 11 January 2005)

Heteroepitaxial CeO_2 (80 nm)/ $\text{L}_{0.67}\text{Ca}_{0.33}\text{MnO}_3$ (400 nm) film structures have been pulsed laser deposited on LaAlO_3 (001) single crystals to fabricate two terminal resistance switching devices. $\text{Ag}/\text{CeO}_2/\text{L}_{0.67}\text{Ca}_{0.33}\text{MnO}_3$ junctions exhibit reproducible switching between a high resistance state (HRS) with insulating properties and a semiconducting or metallic low resistance state (LRS) with resistance ratios up to 10^5 . Reversible electrical switching is a polar effect achievable both in continuous sweeping mode and in the pulse regime. Successive temperature crossover of electronic transport from the thermal activation of the deep levels ($E_a=320$ meV) at high temperatures to thermal activation of the shallow levels ($E_a=40$ meV) and finally at low temperatures to the regime of temperature independent resistance, usually associated with quantum tunneling, has been found for the insulating HRS. The temperature dependence of the LRS reveals a para-to-ferromagnetic phase transition in the $\text{L}_{0.67}\text{Ca}_{0.33}\text{MnO}_3$ (LCMO) electrode at $T_c=260$ K and an anomaly at lower temperatures ~ 200 K corresponding to the Curie temperature of the Mn^{4+} depleted part of the LCMO film. Current-voltage characteristics in the LRS are highly nonlinear, and show negative differential conductivity (NDC). We suggest that the reversible resistance switching occurs due to the electric field induced nucleation of filament-type conducting valence-shifted CeO_x domains inside the insulating CeO_2 matrix. The abrupt insulator-to-metal transition is the result of localization of $4f$ electronic states in Ce^{3+} ions and the subsequent appearance of hole conductivity in the oxygen p -bands. NDC at low temperatures is relied upon the interband scattering of CeO_x carriers from a low energy, high mobility valley into a high energy valley with low mobility.

DOI: 10.1103/PhysRevB.71.045305

PACS number(s): 73.40.Qv, 71.30.+h, 71.28.+d, 72.20.-i

I. INTRODUCTION

Developing a two-terminal nonvolatile memory controlled by voltage and current has been a long standing challenge. Early research efforts focused on switching between amorphous (high resistance) and crystalline (low resistance) states in semiconductors,¹ by joule heating and cooling. Resistance switching due to a current controlled phase transitions was observed in crystalline VO_2 ,² and thin film sandwiches of polymer films show metastable switching due to joule heating.³ Metastable switching was also observed in ZnSe-Ge heterojunctions,⁴ and switching due to order-disorder transitions on the molecular scale was recently found in polymer complexes.⁵ Despite these efforts an industrially viable nonvolatile two-terminal device fulfilling bistable voltage controlled switching was lacking.

In 2000, Liu *et al.* reported that $\text{Pr}_{0.7}\text{Ca}_{0.3}\text{MnO}_3/\text{YBa}_2\text{Cu}_3\text{O}_{7-\delta}$ heterostructures with Ag electrodes exhibited reversible, polarity dependent switching by application of short voltage pulses.⁶ Subsequent work showed that most any perovskite could replace $\text{Pr}_{0.7}\text{Ca}_{0.3}\text{MnO}_3$ (PCMO), that multilevel switching was feasible and that conventional CMOS technology could be used in fabrication.⁷⁻⁹ The actual switching mechanism was later shown to be located on the Ag/PCMO interface, possibly due to ion migration, ruling out the initial idea that this is a bulk PCMO effect.¹⁰ Similar switching effects in Ag/manganite point contacts has been found by Tulina *et al.*,¹¹ where they speculated that switching is due to a current driven phase separation in an oxygen depleted surface layer of the manganite. By introducing a doped insulating layer between the top metal and the conducting oxide, Beck *et al.* showed switching by pulsed, as well as by continuously applied voltage in junctions where

the insulator is a perovskite.¹²⁻¹⁵ The memory effect was explained within the Simmons-Verderber model,¹⁶ where switching is due to storage (high resistance) and release (low resistance) of charges in traps in the insulator. It was also shown that the current density between the top and bottom electrode is not uniform but concentrated in a few filamentary paths which are turned on and off during switching.¹⁵

Although no insulating layer is used in Refs. 7-10, it has been shown that in certain metal-manganite contacts oxygen is depleted from the manganite surface to form an oxidized metal layer between metal and manganite.¹⁷ This layer may thus act as an intrinsic insulating barrier. A degraded manganite surface is indeed found in the manganite-based switching structure in Ref. 11. Alternatively, the degraded surface layer may in itself serve as an insulating layer.

In our view, apart from their memory capabilities, all these structures thus involve oxide materials and have a metal-insulator-oxide build-up. The physics of this class of resistance random access memory (RRAM) structures is not yet fully understood. Earlier switching devices as described above relied on different phase transitions, such as amorphous-crystalline,¹ and order-disorder.⁵ Other resistance change devices rely on, e.g., ferroelectricity. These physical origins of switching can be ruled out for this new class of structures due to the choice of materials (nonferroelectric), due to the absence of (known) ordering phenomena, and due to the polarity dependence which is not compatible with joule heating. Since switching effects exists in contacts of very different area grain boundary effects are also ruled out.¹⁴

A recent model for the polar switching and memory retention in RRAM devices was put forth by Rozenberg *et al.* in which it is assumed that the insulator contains metallic

domains of two distinct types: a number of smaller domains close to the interfaces and a single large bulk domain.¹⁸ During switching the occupation of the interface domains changes and subsequently the tunneling rates in and out of these domains changes.

To elucidate the roles of the conducting bottom layer and the insulating barrier in the family of two-terminal RRAM devices we have fabricated and characterized novel metal/oxide-insulator/oxide-conductor (MOC) three-layer Ag/CeO₂/L_{0.67}Ca_{0.33}MnO₃/LaAlO₃(001) structures exhibiting reproducible switching between a low resistance state (LRS) and a high resistance state (HRS) with resistance ratios up to 10⁵. By inserting a very thick insulating CeO₂ layer, 80 nm, we have succeeded to differentiate between interface and bulk effects in the insulator.

Switching between the HRS and the LRS is obtained by the application of a positive and negative threshold voltage, or by repeated positive and negative pulses for the HRS and the LRS, respectively. Hereafter positive voltage corresponds to a positive bias applied to the top Ag electrode. The nature of the low and high resistance state is probed by extensive transport measurements as a function of temperature and magnetic field. Loss tangent measurements show that the LRS at room temperature is successfully modeled as a very leaky capacitor (low-Ohmic resistor and capacitor connected in parallel). The HRS on the other hand, behaves as a high quality capacitor with highly resistive electrodes. Huge differences in resistance and frequency behavior between HRS and LRS indicate that LCMO surface effects cannot account for switching in this case and that insulator transport is the dominating mechanism.

Activated temperature dependence of the resistance in the HRS is found down to ~100 K below which resistance does not increase and quantum tunneling is the dominating transport mechanism. In the LRS, double peaks in *R* vs *T* are found, corresponding to the Curie temperature of bulk, and a Mn⁴⁺-depleted part of L_{0.67}Ca_{0.33}MnO₃ (LCMO) film, respectively. Furthermore, below the ferromagnetic transition temperature of bulk LCMO at ~260 K, strongly magnetic field dependent nonlinearities in the *IV*-characteristics appear. The negative differential conductivity (NDC) suggests that this is due to scattering of carriers from a low energy, high mobility valley to a high energy, low mobility valley in the band structure of the conducting filaments.

The mixed valence property of the insulating barrier is thought to be crucial for the switching property of the MOC junction. Current conducting filamentary paths are nucleated at the CeO₂/LCMO cathode interface whereas a corresponding reverse voltage cures the insulating barrier converting these filaments from the metallic to the insulating state. We suggest that the electric field induced electron transport in CeO₂ is a hole conductivity in the oxygen *p*-band which appears due to a valence shift in cerium from 4+ to 3+ resulting in the localization of Ce 4*f*-states. This model explains the polar character of the switching effect as well as the magnetic nature of the conducting CeO_x filaments.

II. PROCESSING TECHNIQUE AND STRUCTURAL CHARACTERIZATION

The fabrication of the test structures was carried out according to the outline below. Ceramic targets with the com-

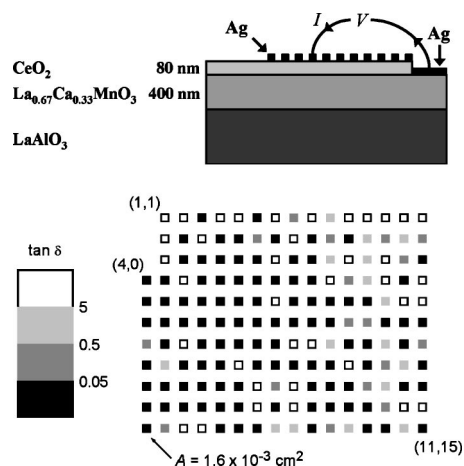


FIG. 1. Upper panel: Schematic side view of the CeO₂/LCMO structure deposited on a LaAlO₃ substrate with black indicating silver contacts. Lower panel: Schematic top view of contact matrix. Specific contacts are identified by number pairs where the first number is the vertical position in the matrix and the second number is the horizontal position. Quality of dielectric barrier, i.e. $\tan \delta$ at 10 kHz, is indicated by the grey scale. Only results from measurements on points with $\delta < 0.05$ (black) are presented in this paper.

positions L_{0.67}Ca_{0.33}MnO₃ and CeO₂ were ablated using a 248 nm KrF excimer Lambda Physik-Compex-102 laser with a radiation energy density of 5 J/cm², a pulse repetition rate of 20 Hz and a substrate-to-target distance of 60 mm. The deposition onto the LaAlO₃(001) (LAO) single crystal was carried out at an oxygen pressure of 250 mTorr, with a substrate temperature of 730 °C for LCMO and 750 °C for CeO₂. The structure was finally postannealed *in situ* at 400 mTorr oxygen for 10 min. Measured layer thicknesses were approximately 400 nm and 80 nm for LCMO and CeO₂, respectively.

An 11 × 16 matrix of 0.4 mm × 0.4 mm silver top electrodes separated by a 0.25 mm gap was evaporated onto the CeO₂ top layer and a 10 mm × 1 mm silver bottom electrode was evaporated onto the exposed LCMO (see Fig. 1).

The structure was mounted on a 16 mm × 10 mm polycor substrate with thermally conducting paste and gold wires were attached with silver paint (Du Pont 5504) to selected contacts and to larger contact pads on the polycor substrate. After heating the sample at 150 °C for ~15 min the silver contacts were mechanically stable. The heating serves the extra purpose of restoring junctions to the virgin state, i.e. close to the HRS. Throughout this paper, the words contact and junction are used interchangeably to refer to the system of one silver contact and the column of CeO₂/LCMO directly below. Contacts are labeled (*y*,*x*) with *y*(*x*) indicating the vertical (horizontal) position in the contact matrix as shown in Fig. 1.

X-ray diffraction measurements on a structure identical to that used for *IV*-tests were performed to determine the crystalline quality and phase purity of the CeO₂/LCMO bilayer on LAO. The absence of any peaks except (00*l*) in the θ - 2 θ scan and rocking curves (ω -scans) with FWHMs of

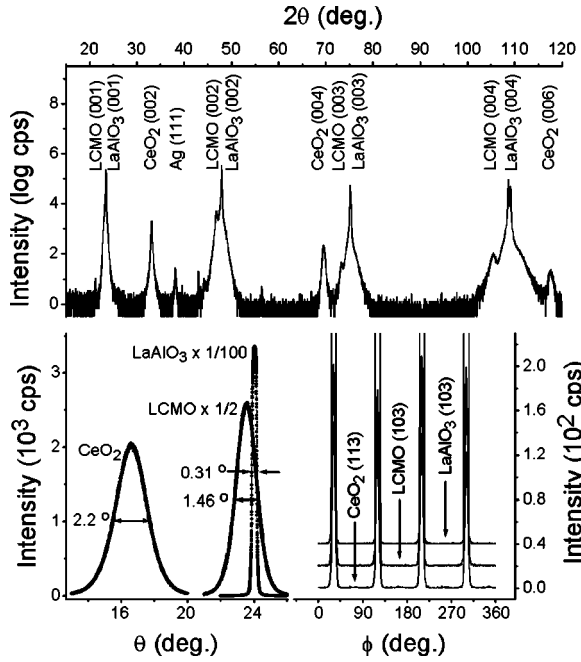


FIG. 2. X-ray diffraction patterns from CeO₂/LCMO/LAO structure showing the θ - 2θ scan (upper panel), rocking curves of (002) Bragg reflections (lower left panel), and ϕ -scans (lower right panel) of off-normal (113)- and (103)-planes at the oblique geometry: $\theta_{\text{sample}}=53.55^\circ, 57.64^\circ, 58.43^\circ$; $2\theta_{\text{detector}}=56.46^\circ, 78.15^\circ, 80.01^\circ$ for CeO₂, LCMO and LAO, respectively.

0.31°, 1.46°, and 2.2° for LaAlO₃, LCMO, and CeO₂, respectively, as shown in Fig. 2, indicate an exclusive c -axis orientation of the CeO₂/LCMO bilayer. Some crystalline clusters exist in residual silver paste as evident from the low intensity Ag(111) peak. With optimization of deposition parameters the epitaxy could be much improved but that was not the goal of the present study. Due to the small lattice mismatch between the face diagonal of the LCMO cubic cell and the side of CeO₂ (0.26%) it is expected that the two layers grow with a side-on-diagonal orientation. This prediction is confirmed by the coincidence of reflection peaks in the ϕ -scan of LCMO and LAO (103) planes and CeO₂ (113) planes (Fig. 2). The fourfold symmetry and absence of additional peaks also indicate excellent in-plane texture.

In addition to x-ray diffraction the insulating quality of the CeO₂ layer has been quantified by dielectric spectroscopy of the Ag/CeO₂/LCMO capacitors (see Fig. 3). Low $\tan \delta$ indicates low dielectric losses and if current transport across the insulator is determined by defect density one can use $\tan \delta$ as a characteristic of dielectric quality. The ratio of resistances in HRS and LRS decreases with increasing $\tan \delta$ and no switching occurs above a certain limit. Good switching, with resistance ratios in the range 10^3 – 10^5 , occurs for the contacts with $\tan \delta < 0.05$ marked with a black color in Fig. 1. Figure 3 shows the frequency dispersion of $\tan \delta$ in the HRS and the LRS. Modeling our system by the equivalent circuit consisting of one resistor R_{LCMO} connected in series to a parallel connected capacitance C and resistor R_{CeO_2} gives the frequency dependence

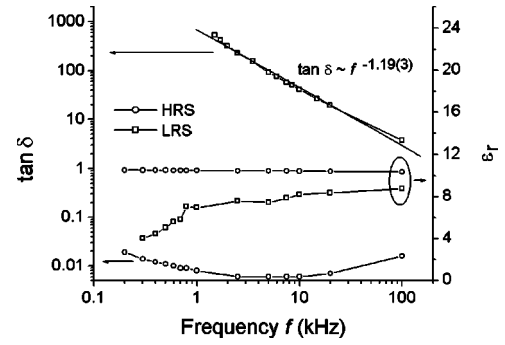


FIG. 3. Frequency dependence of $\tan \delta$ and ϵ_r in contact (4,9) in the HRS (circles) and LRS (squares). The $\tan \delta$ in the LRS follows a power law dependence, $\tan \delta \propto f^{-1.19(3)}$ while it exhibits a minimum in the HRS as predicted by Eqs. (1)–(3). Capacitance (and thus ϵ_r) in the HRS exhibits a weak logarithmic frequency dispersion, $C \propto \log 1/f$.

$$\tan \delta = \frac{1 + (2\pi f C)^2 R_{\text{LCMO}} R_{\text{CeO}_2} + R_{\text{LCMO}}/R_{\text{CeO}_2}}{2\pi f C R_{\text{CeO}_2}}, \quad (1)$$

where R_{LCMO} includes both bulk and interface resistance. For small insulator resistance

$$2\pi f C R_{\text{CeO}_2} < 1, \quad (2)$$

the frequency dependent term in the nominator of Eq. (1) can be neglected, which is consistent with the behavior $\tan \delta \propto f^{-1.2}$, found experimentally in the LRS.

In the HRS, the insulator resistance is large and Eq. (1) with $R_{\text{LCMO}}=1$ k Ω (estimated), $C=180$ pF and $R_{\text{CeO}_2}=100$ M Ω predicts that $\tan \delta$ should have a minimum at the frequency,

$$f_{\text{min}} = \frac{\sqrt{1 + R_{\text{CeO}_2}/R_{\text{LCMO}}}}{2\pi R_{\text{CeO}_2} C} \approx 3 \text{ kHz} \quad (3)$$

which is close to the observed value in Fig. 3.

A crude estimate of the relative dielectric constant ϵ_r of the CeO₂ can be obtained by approximating our junctions as parallel plate capacitors with area $A=1.6 \cdot 10^{-3}$ cm² and thickness of the dielectric $t_{\text{CeO}_2}=80$ nm. Using the asymptotic form of Eq. (1) at Eq. (2) and measured values of the resistance of the junction in the LRS we obtain $\epsilon_r^{\text{LRS}}=4$ –9. In the HRS the capacitance is measured directly by the LCR-meter and $\epsilon_r^{\text{HRS}}=10$ –11 is found, with a weak logarithmic frequency dependence. These values are in agreement with previous measurements on high quality CeO₂/Si films under similar conditions.¹⁹

Consequently, the behavior in both the HRS and the LRS are consistent with the equivalent circuit model where switching changes R_{CeO_2} dramatically. Small differences in the dielectric constants, and hence C , in the HRS and the LRS could be related to a higher defect density in the LRS.

III. SWITCHING

Using a Keithley 2004 Sourceter, 2-point IV-characteristics between selected top contacts and the

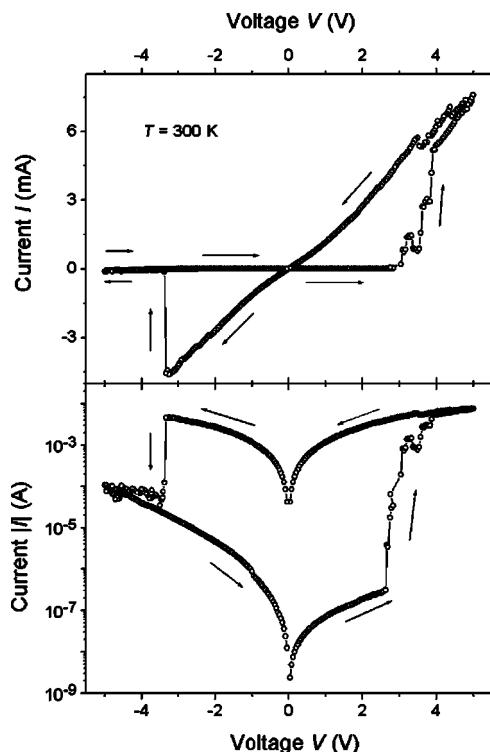


FIG. 4. IV -characteristics (upper panel) and $\log|I|$ vs V (lower panel) of contact (6,1) at room temperature with arrows indicating the direction of the sweep.

larger ground contact were recorded in *voltage control mode*. Positive voltage corresponds to a positive bias applied on the top electrode. Starting from a high resistance state (HRS) the voltage was swept and at some threshold value, typically a few volts, the resistance decreased sharply, by several orders of magnitude as illustrated in Fig. 4. Further sweeping to even higher voltages further decreases the resistance but not as dramatic as close to the switching voltage.

Sweeping the voltage back to negative voltages the low resistance state (LRS) is stable until the negative threshold voltage is overcome, whereby the resistance increases sharply. Further increasing the negative bias can further increase resistance but at too high negative voltages the structure will break down and switching properties are lost. The negative switching voltage is related to the maximum positive voltage that was reached when switching to the LRS.

There is no switching if the threshold voltage is not overcome, thus the IV -characteristics have reversible character. Note also that switching from the HRS to the LRS *only occurs* when positive bias is applied to the top electrode. Similarly, switching from the LRS to the HRS only occurs when negative bias is applied to the top electrode. This means that the IV -curve shown in Fig. 4 cannot be reproduced when sweeping the voltage in the opposite direction of the arrows. Based on these observations electrical switching in $\text{Ag}/\text{CeO}_2/\text{L}_{0.67}\text{Ca}_{0.33}\text{MnO}_3$ junctions must be classified as a *reversible polar effect*.

The above described continuous and reproducible resistance switching is qualitatively the same in all contacts with possible resistance ratios ranging from 1 to 100 000. The

resistance states denoted HRS and LRS should not be regarded as two distinct discrete levels since a continuum of resistance states from the extreme HRS to the extreme LRS exist. This is why such a wide range of switching ratios is possible. In this paper, the HRS and LRS will denote two states with qualitatively different temperature dependence and low temperature properties with switching resistance ratios above 10^3 .

There are two asymmetries in the IV -characteristics of a typical junction. First, the switching to and from the LRS is generally not symmetric with the general tendency being that the initial switch to the LRS requires lower voltage than the switch to the HRS. Second, as evident from Fig. 4, it seems that there also exists a difference between the positive and negative branches of the two states. The initial (positive branch) HRS has got higher resistance as compared with the second (negative branch) HRS.

Since switching is polarity dependent and the junction is not symmetric one would not expect switching to be completely symmetric. Differences between positive and negative threshold voltages can be related on the built-in electrical fields both at the $\text{Ag}-\text{CeO}_2$ and $\text{CeO}_2\text{-LCMO}$ interfaces.

The second asymmetry is only apparent since the HRS in the negative branch of Fig. 4 is not the same as the HRS in the positive branch. No asymmetry is visible if we simply probe the LRS or HRS by sweeping the voltage from zero to voltages well below the positive and negative switching thresholds as shown in Fig. 5. The lower resistance of the negative branch HRS is due to the first asymmetry as explained above. Applying a larger negative voltage would result in a negative branch HRS closer to the positive branch HRS.

To reach stable LRS and HRS suitable for probing it is more convenient to use short voltage pulses to switch the junction rather than the “continuous sweep” described above. Pulsing allows for higher voltages to be used without the risk of destroying the contact. Pulsed current was supplied by an AVTECH-1010-C pulse generator forming rectangular pulses with amplitudes in the range 1–10 V and with typical widths 100 ns–10 ms. A general observation is that switching seems to be related to the total charge so that with lower voltages, wider pulses or a larger number of pulses are needed. The magnitude and duration of the pulses are however not critical parameters for switching to occur. By applying several pulses in series the structure was switched and IV -characteristics could be measured as shown in Fig. 5. The positive and negative branches are perfectly symmetric and the differential resistance $\mathcal{R} = dV/dI$ at zero bias for the junction (11,0) was about 36 M Ω in the HRS and 1.4 k Ω in the LRS, a difference of more than four orders of magnitude. The voltage dependence which is almost Ohmic at room temperature, can be fitted to

$$I(V) = \frac{V}{R_0} \left(1 + \left(\frac{V}{V_0} \right)^2 \right), \quad (4)$$

in both the HRS and the LRS but the nonlinearity is larger in the HRS, $V_0^{\text{LRS}}/V_0^{\text{HRS}} = 1.6$, so the voltage dependence is not universal. For low voltages Eq. (4) follows the current-voltage relation ascertained by Simmons and Verderber.¹⁶

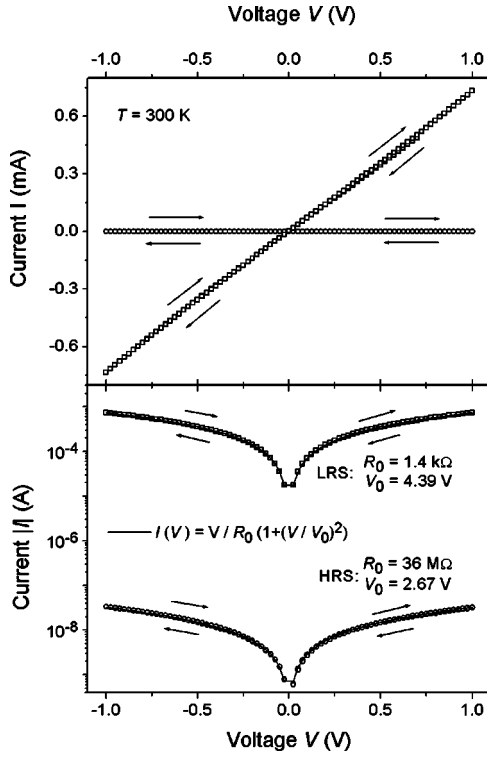


FIG. 5. IV -characteristics (upper panel) and $\log|I|$ vs V (lower panel) of the HRS (circles) and the LRS (squares) of contact (11,0) at room temperature after using pulsed current to switch the contact. Solid lines are fits to $I(V) = V/R_0(1+(V/V_0)^2)$ with $R_0^{\text{HRS}} = 35.6(2) \text{ M}\Omega$, $V_0^{\text{HRS}} = 2.67 \text{ V}$, and $R_0^{\text{LRS}} = 1.428(3) \text{ k}\Omega$, $V_0^{\text{LRS}} = 4.39 \text{ V}$.

$$I(V) = \frac{1}{\sqrt{6}} \frac{V_0}{R_0} \sinh\left(\sqrt{6} \frac{V}{V_0}\right). \quad (5)$$

IV. THE HIGH RESISTANCE STATE

Using a closed cycle cryostat the temperature of the sample was varied between 15 K and 300 K while using the above mentioned setup for IV -measurements. A sequence of IV -characteristics at different temperatures is presented in Fig. 6. Figure 7 shows differential resistance as a function of temperature and current in the HRS. Differential resistance dV/dI derived from IV -measurements are henceforth denoted by \mathcal{R} while measured resistance V/I is denoted by R . The resistance followed an activated temperature dependence

$$\mathcal{R} \propto \exp\left(\frac{E_a}{k_B T}\right) \quad (6)$$

between 250 K and 75 K, with the activation energy $E_a = 40 \text{ meV}$, as indicated by the Arrhenius plot in Fig. 7. This corresponds to thermal activation of shallow trapped charge levels in the CeO_2 film. At higher temperatures, although only two data points are available, we find $E_a = 320 \text{ meV}$ thus indicating crossover of the thermal activation process from the shallow to deep levels in CeO_2 . Below 75 K–100 K the resistance deviates from activation behavior and ends to

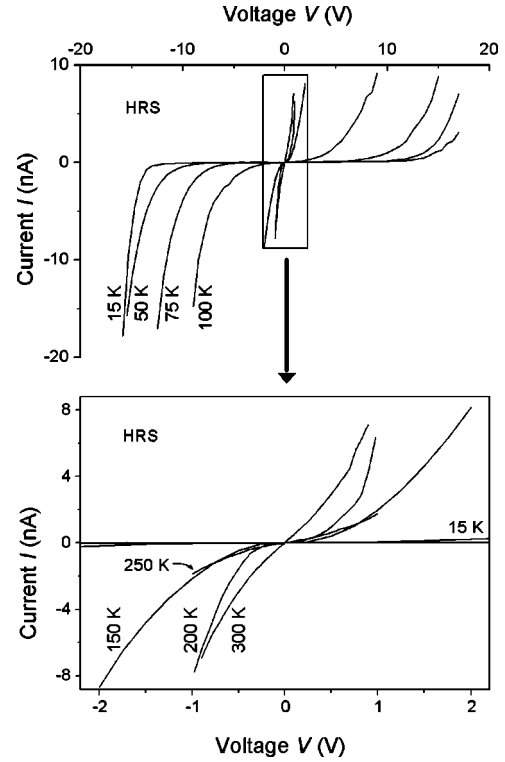


FIG. 6. Upper panel: IV -characteristics in HRS of contact (6,1). Lower panel: Enlargement of boxed portion in upper panel.

grow at low temperatures. The (absence of) temperature dependence indicates that this is the Fowler-Nordheim regime of quantum tunneling as typical for insulator transport at low temperatures.

Previous measurements on CeO_2/Si have shown the activation character of electron transport for temperatures above $\sim 200 \text{ K}$ with an activation energy in the range 200–400 meV,^{20–22} and temperature independent tunneling at lower temperatures.²² Our results for the CeO_2 /manganite system thus deviate from previous results on metal/oxide/semiconductor (MOS) structures in the temperature range 75–250 K. Note that this corresponds to temperatures below the para-to-ferromagnetic transition of LCMO, possibly indicating effects of spin-polarization from the ferromagnetic bottom electrode.

The stable defects in CeO_2 expected to increase leakage currents in the HRS are mainly doubly charged oxygen ion vacancies with Ce^{3+} -ions.²⁰ Pure tetravalent $\text{Ce}^{4+}\text{O}_2^{2-}$ is non-magnetic and the weak paramagnetism exhibited in real samples is ascribed to a low concentration of such impurities. A larger ionic radius of Ce^{3+} (1.13 Å compared to 0.97 Å for Ce^{4+}) works also in the same direction, compensating the free volume emptied by volatile oxygen. Later we will bring additional arguments showing that the valence shift in CeO_2 may supply carriers to form a narrow conducting band and thus influence the transport properties in the insulating barrier.

V. THE LOW RESISTANCE STATE

To determine whether the junctions are magnetically active at room temperature IV -characteristics were traced under

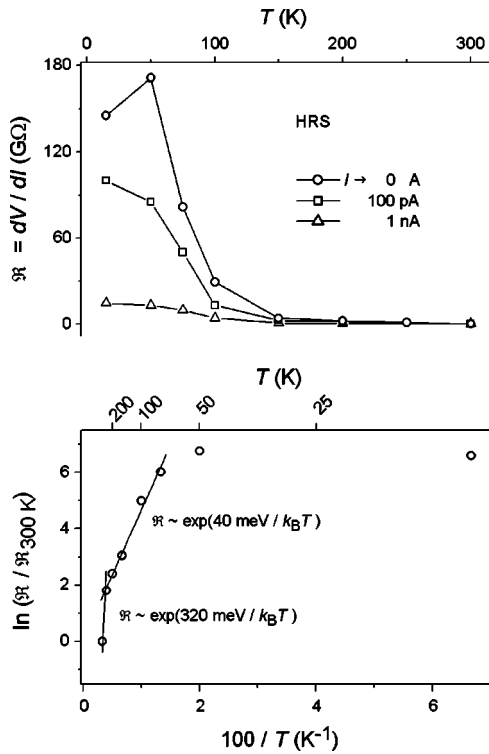


FIG. 7. Upper panel: Temperature dependence of differential resistance $\mathcal{R} = dV/dI$ at different bias in the HRS of contact (6,1) as derived from IV -measurements (Fig. 6). Lower panel: Arrhenius plot of differential resistance (asymptotic at $I \rightarrow 0$) vs temperature (circles). The upper solid line is a linear least squares fit to $\mathcal{R} \propto \exp(E_a/(k_B T))$, with the result $E_a = 40$ meV, for data in the range of 75 K to 250 K. Fitting the same function to the data points at $T = 250$ K and $T = 300$ K yields the lower solid line, and the obtained activation energy $E_a = 320$ meV is equal to previous recorded values for bulk CeO_2 in this temperature range.

applied magnetic field. Magnetic measurements were performed in an Oxford Instruments cryostat, down to 77 K, in a Varian electromagnet capable of magnetic fields H up to 20 kOe. The sample could be rotated to align the field H in-plane and out-of-plane with respect to the film surface. No significant effects of the magnetic field exist at room temperature, regardless of orientation (not shown). Neither switching thresholds nor the resistance are affected, ruling out the possibility that spin-polarization or other magnetic effects are the paramount reason for the switching phenomenon.

At low temperatures a number of new features in the LRS of the $\text{Ag}/\text{CeO}_2/\text{LCMO}$ junction appear. The temperature dependence of the resistance in the LRS was measured in *constant current mode* in the low current regime as shown in the upper panel of Fig. 8 for one contact in different low resistance states obtained after different switching voltages were applied. In addition to the resistance peak associated with the ferromagnetic transition in the interior of LCMO film at $T = 260$ K, there is a second peak observed at a lower temperature T_{cs} . Qualitatively, all contacts in the LRS have this double peak feature in the RT -characteristics. While T_c is

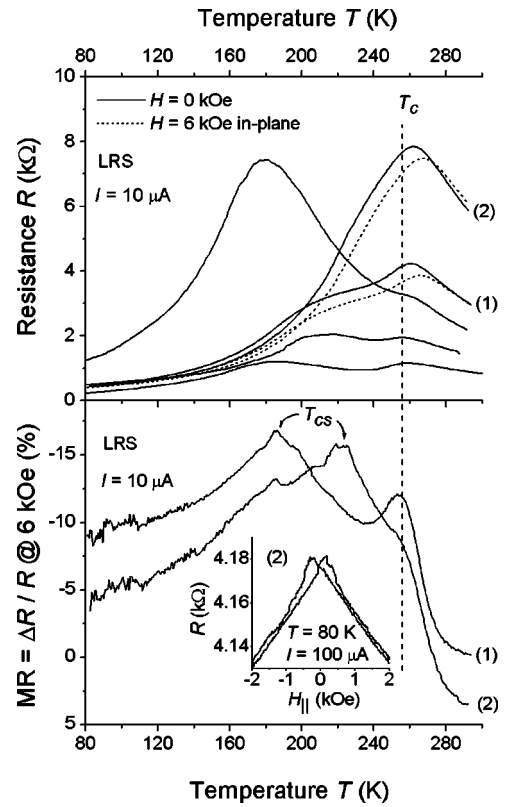


FIG. 8. Temperature and magnetic field dependence of resistance in LRS measured in *constant current mode* in contact (11,15). Upper panel: Resistance at $I = 10 \mu\text{A}$ in a few different LRS and magnetic field dependence for states labeled (1) and (2). Lower panel: Magnetoresistance at $H = 6$ kOe measured with $I = 10 \mu\text{A}$ in the states (1) and (2). Inset: Resistance vs magnetic field measured at 100 μA and 80 K in state (2).

constant for the selected contact, as it should be, the magnitude, shape and position T_{cs} of the second peak varies with voltage history. Resistance as a function of magnetic field measured at temperatures below this second peak shows the standard CMR behavior associated with LCMO below the paramagnetic-to-ferromagnetic transition (see inset of lower panel of Fig. 8). Significant magnetoresistance measured below T_{cs} (thus far away from the “bulk” T_c), as shown in the lower panel of Fig. 8, also suggests that T_{cs} corresponds to a para-to-ferromagnetic transition in the oxygen depleted part of LCMO surface layer.

Electron-beam induced current measurements performed by Rossel *et al.* clearly showed that switching in the RRAM structures is due to the activation and deactivation of filamentary current paths within the otherwise insulating medium.¹⁵ Asserting that such paths are responsible for the transport through the insulator we conclude that T_{cs} is the effective Curie temperature of the LCMO surface region where the current paths meet the LCMO. The magnetoresistance ratio defined as

$$\text{MR} \equiv \frac{\Delta R}{R} = \frac{R(H)}{R(0)} - 1 \quad (7)$$

shown in the lower panel of Fig. 8 supports this claim with a

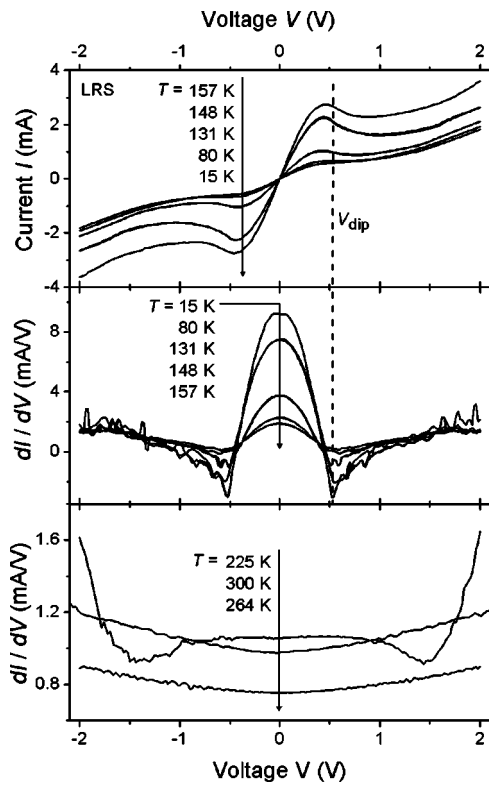


FIG. 9. IV -characteristics in LRS of contact (10,12) at low temperatures. Upper panel: IV -characteristics at temperatures well below the para-to-ferromagnetic transition. The given temperatures, from top to bottom, correspond to the order of curves when moving in the direction of the arrow. Middle panel: Differential conductance as calculated from IV -curves in upper panel. Lower panel: Differential conductance for higher temperatures where nonlinearities are not as pronounced.

broadened second MR peak due to a distribution of T_{cs} 's, and some fine structure due to competing current paths.

IV -characteristics in the LRS are highly nonlinear for temperatures below the ferromagnetic transition at $T_c = 260$ K. It is important to note that there is no qualitative change in the IV -characteristics when passing through the second anomaly at T_{cs} , except for the absolute magnitude of the conductivity. The differential conductance $\partial I / \partial V$ in the LRS as calculated from IV -characteristics is shown in Fig. 9. IV -characteristics, recorded in *constant voltage mode*, show the presence of three different transport mechanisms. For small voltages the differential resistance is very low, stable and gradually increases with increasing voltage. At a certain voltage $V_{NDC} \approx 0.5$ V, there is a transition from the stable low resistance state to a more noisy high resistance state. Between these two states there is a region with NDC whose magnitude has a local extremum at V_{NDC} . Hysteresis regions may appear when sweeping voltage up and down close to this region and in certain cases this hysteresis may be very large as shown in the lower panel of Fig. 10. Sweeping the voltage to values above the threshold voltages changes zero bias resistance, the exact shape of the IV -characteristic and the exact position of the anomalies (compare the upper and

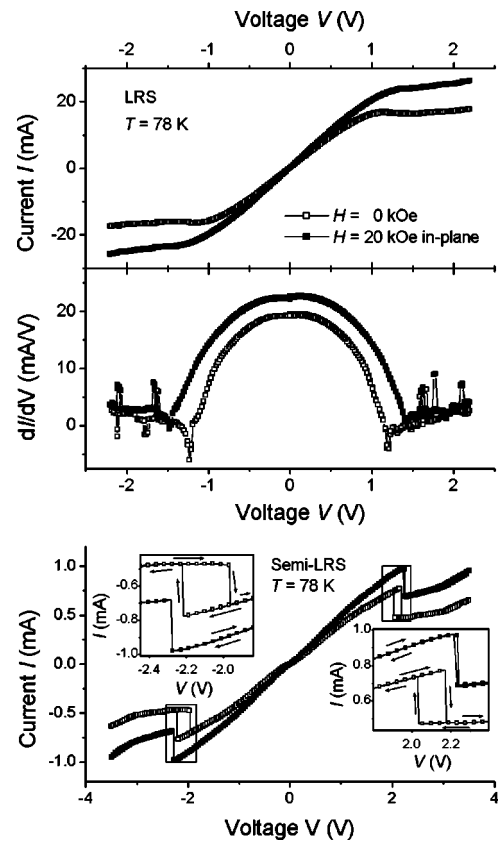


FIG. 10. Upper panel: IV -characteristics in LRS of contact (6,14) for in-plane fields $H_{\parallel} = 0$ (filled squares) and $H_{\parallel} = 20$ kOe (open squares). Middle panel: Differential conductance dI/dV as calculated from IV -curves in upper panel. Lower panel: IV -characteristics in a LRS of contact (6,14) with larger zero bias resistance. Insets show magnified portions of boxed portions detailing the hysteretic behavior.

lower panels of Fig. 10). However, the region with a negative $\partial I / \partial V$ is always present in the LRS at low temperatures. As the effects are not observed in LCMO films the insulating layer and/or the degraded surface layer is pivotal in obtaining the NDC effect. Similar anomalies in the IV -characteristics have also been found in Ag/manganite point contact junctions.²³

It was mentioned that there were no magnetic effects at room temperature in either the HRS or the LRS. At low temperatures a magnetic field still does not affect the HRS whereas the LRS exhibit two features: at 20 kOe there is a $\delta V = V_{NDC}(H) - V_{NDC}(0) = 0.1 - 0.3$ V shift of the NDC anomaly to higher voltages as well as an increase in conductivity, i.e., negative magnetoresistance, typical of CMR materials. It seems also that the application of a magnetic field eliminates the lability boundaries (hysteresis) of the NDC-effect as shown in the lower panel of Fig. 10.

As the specific features, $V_{NDC}(H)$ of the IV -anomalies are strongly dependent on voltage history it is relied upon the current path within the insulator and LCMO surface layer, and not upon the bulk LCMO. The activation voltages V_{NDC} are too large to correspond to any elementary excitation (e.g.,

magnons in LCMO),²⁴ and local overheating effects due to highly resistive grain boundaries in the manganite, as observed by Todd *et al.*,²⁵ can be excluded by the following arguments.

A resistance increase due to local overheating of LCMO would correspond to moving towards higher T in the RT -curve associated with bulk LCMO. The influence of Joule heat on an Ag/LCMO/LAO film structure identical to the device under study, except for the absence of a CeO_2 isolating barrier, was investigated. We found that at a released electrical Joule heat of 40 mW (the same range of heat observed at the position of the NDC in Fig. 10) and at 78 K, the temperature of the film increases only about 0.8–1 K. Of course, we consider some average temperature deviation while locally such an increase could be higher for a fast voltage scan. But the acquisition time between points, from 100 ms to 3000 ms, is nonetheless 2–3 orders of magnitude higher than the relaxation time for manganite film-to-substrate heat exchange as shown by Lisauskas *et al.*²⁶ So, even if some fast effects in our structures exist we cannot detect them with the technique that was used.

We also consider the IV -curves shown in Fig. 10 in detail. As mentioned above the relaxation is fast compared to the acquisition time and we may consider any heat delivered into the heterostructure to spread rapidly. If NDC is triggered by a critical amount of Joule heat in the LCMO we should expect the peak values of NDC to occur at the same level of heating. However the peak occurs at 20 mW of applied electrical power at zero magnetic field ($H=0$) and 34 mW at $H=20$ kOe. Furthermore, since the delivered heat in voltage control mode can be written as $P=V^2/R$, the shift with magnetic field due to the negative magnetoresistance of LCMO should be in the opposite direction than what is observed.

On the basis of these considerations, local overheating of LCMO can be excluded and an explanation of their origin, relying on overheating in CeO_2 is suggested below.

Negative resistance in III–V semiconductors with n -doping have been known since the discovery of the Gunn effect in GaAs and InP in 1963,²⁷ and is now well understood.²⁸ The negative resistance found in these compounds is an effect of the band structure which exhibits a conduction band with a low energy, high mobility central valley and a high energy, low mobility side valley. At zero bias only the low energy valley is populated but as the electrical field is increased above some critical value carriers will transfer to the low mobility valley leading to negative conductivity. The differential resistivity of such a material will thus start positive, and then tend to negative values as the field passes the critical value and will eventually become positive again as carriers are transferred to other high mobility regions. Note that the NDC effect described above is valid for both electrons and holes.²⁹

Asserting that CeO_x conducting filaments fulfill the requirement of high- and low mobility oxygen p -band valleys in the Brillouin zone separated by a fraction of an eV, we can rely our observation of the NDC phenomenon on the “hot holes” effect outlined above. Although the band structures of CeO, CeO_2 , and Ce_2O_3 are known and do indeed exhibit

multivalleyed band structure,^{30,31} we do not know the band structure of the valence shifted conducting filaments which remains to be explored.

The shift of V_{NDC} with magnetic field can be attributed to magnetic effects in CeO_2 . The onset of NDC is determined by a critical amount of the Joule heat

$$\delta W = I_{\text{NDC}} V_{\text{NDC}} \tau_E, \quad (8)$$

accumulated in the electronic subsystem, where τ_E is the energy relaxation time.³² As shown in Fig. 10, in a magnetic field $H=20$ kOe the NDC-effect occurs at higher current (24 mA compared to 17 mA at $H=0$) and higher voltage $V_{\text{NDC}}(H) - V_{\text{NDC}}(0) = 0.3$ V. We suggest that the additional Joule heat in the form of Eq. (8) is required to compensate for an effective Zeeman energy shift, $\delta W = \mu B$, in magnetic $4f$ Ce^{3+} core states in the conducting filaments. Comparing the Zeeman energy with the increase in delivered heat, using the typical energy relaxation time $\tau_E = 10^{-13}$ s we conclude that about $8 \cdot 10^7$ Bohr magnetons, corresponding to $3 \cdot 10^7 \text{Ce}^{3+}$ ions with localized f -electrons, form the conducting channel in the $\text{Ag}/\text{CeO}_2\text{L}_{0.67}\text{Ca}_{0.33}\text{MnO}_3$ junction. Although this is a very crude estimate, with τ_E not even known to one order of magnitude, this corresponds to a single filament with the lateral size 0.2 μm , in agreement with earlier observations.¹⁵

Tulina *et al.*, in experiments with the direct Ag-manganite point contacts, did not observe any magnetic field dependence of the conductance up to 40 kOe.²³ This fact is in line with both models proposed above if either (i) the bulk LCMO resistance is negligible in comparison with the junction resistance or (ii), the number of “hot” magnetic carriers in the much thinner insulating layer is too small to visualize the effect.

In the LRS, the LCMO bottom electrode and its magnetoresistance is certainly contributing to the conductivity of a bottom electrode and thus complicating the analysis of the junction characteristics. By patterning the CeO_2 -LCMO bilayer with very narrow and thin LCMO channels, and thus introducing a *three-terminal device*, such effects can be reduced. However the CeO_2 -LCMO interface and LCMO surface region would still be included and these are the regions where the most serious deviations from bulk LCMO behavior will occur.

VI. CONCLUSIONS

Extensive transport measurements on $\text{Ag}/\text{CeO}_2/\text{L}_{0.67}\text{Ca}_{0.33}\text{MnO}_3$ heterostructures, a member of a new class of two-terminal resistance switching devices, have revealed a number of novel features that shed light on the physics of these structures. Giant switching resistance ratios achievable in these structures, and the capacitive nature of the HRS, show that switching is achieved within the insulating barrier and not in the manganite. Temperature dependence of resistance further reveals that the conductive paths are semiconducting or metallic as compared to the insulating HRS. Resistance switching is thus an electric field induced metal-insulator transition in the insulating medium.

We propose that switching in the RRAM devices is due to a shift in the valence state of a particular cation in the insulator, and that such a shift nucleates at one interface and propagates through the thickness of the insulator creating a conduction path. This can be regarded as a Mott metal-insulator transition induced by a critical density of additional carriers added by doping. In our case the cation with mixed valence is Ce^{4+}/Ce^{3+} with the tetravalent state representing pure insulating nonmagnetic CeO_2 , and the trivalent state the paramagnetic “acceptor” dopants.

The electronic configuration of the Ce-ion in a close crystalline environment is a cornerstone issue of the proposed model. Cerium sits in the first place in the row of the rare-earth elements. The $4f$ -shell starts to be filled just from the ^{58}Ce atom and there is a strong competition between the $4f$ -, $5d$ -, and $6s$ -electronic states. As a result, the potential well for $4f$ -states in Ce is very shallow and is sensitive to small changes in the crystalline field.

In LCMO the proper concentration of divalent cations (Sr, Ca, Ba, Pb) should substitute La^{3+} to achieve the Mn^{4+} -to- Mn^{3+} ratio required for ferromagnetic ordering (low resistance state). In CeO_2 we believe a similar “doping” with trivalent Ce can be achieved with the application of an electric field. In both LCMO and CeO_2 oxygen vacancies, which are always present in the equilibrium concentration, will disturb the local valence state. The actual switching mechanism in the MOC junction incorporates the effects of mixed valence and oxygen vacancies and is detailed below.

At the CeO_2 -LCMO interface due to the local fluctuation of electrical field oxygen ions can migrate through the transparent interface from the oxide cathode to the insulator and further to the anode. In the manganite, the appearance of oxygen vacancies leads to the local reduction reaction Mn^{4+} -to- Mn^{3+} and results in the local suppression of the ferromagnetic state, lowering the critical temperature and increasing local resistivity. As for the CeO_2 insulator, there is a narrow empty Ce f band in the gap between the valence and conducting bands.³³ When oxygen atoms move diffusively towards the anode, the formation of the oxygen vacancies facilitate simultaneous condensation of two electrons into localized f -level traps on two Ce atoms.³⁴ Therefore, oxygen electromigration might result in the formation of complexes comprising of one oxygen vacancy and two Ce^{3+} ions. Transformation of the Ce $4f$ valence states into the localized core-like electrons occur due to the reorganization of the nearest oxygen neighborhood. In CeO_2 , Ce $4f$ electrons leave the host atoms and are hybridized into the p bands of O atoms. In $Ce_2^{3+}O_3^{2-}$, they come back to the Ce atoms, localized in f states and leave holes in the oxygen p band. Such a valence shift of the cerium oxide will propagate and self-assemble itself under the applied electric field through the insulator until a conductive percolation path of neighboring Ce^{3+} sites is created and an abrupt metal-insulator phase transition occurs when some critical density of valence shifted sites is reached. Once created such a path is stable and reflects the

mixed valence property of the cerium ions. The role of the electrical field is thus to initiate the process of oxygen migration by nucleating a domain of valence shifted sites. When the opposite voltage is applied the reverse oxygen migration from CeO_2 to LCMO shifts the valence of the initial domain back to the original stable configuration and this propagates along the conduction path, effectively turning it off.

The above explanation is supported by a number of facts: the occurrence of the switching phenomenon in materials with mixed valence cations such as Ce, Cr,¹²⁻¹⁵ Pr,⁶ and Mn;⁶⁻¹¹ the preference in using a conducting oxide such as LCMO,^{11,23} YBCO,^{6-8,10} or $SrRuO_3$,^{12,13,15} as the bottom electrode thus ensuring free oxygen migration through this interface; the oxygen (Mn^{4+}) depleted surface layer of the LCMO bottom electrode; the observation that during pulsed switching the product of pulse height I and pulse duration δt , i.e., charge, determines the resistance change, which is consistent with a model of charge transfer; and the increased defect density in the LRS as inferred from capacitive measurements.

Let us estimate the threshold switching voltage, as the last argument in the favor of the Mott transition in the insulating barrier. For this we use the well known experimental fact that the pure Ce metal experiences a high-volume γ to a low-volume α isostructural (fcc) phase transition at a pressure of about 7 kbar. This transition is believed to have an electronic nature and to be associated with the movement of a sharp $4f$ level from below to above the Fermi level, or equivalently, the delocalization of a $4f$ core electron.³⁵⁻³⁸

As stated above, the conductivity in the LRS is induced by a valence shift due to the movement of localized $4f$ -electrons from two neighboring Ce ions to the oxygen p -state. This spatial charge transfer creates the local dipole moment $\pi = 2ed_{Ce-O}$, where the interatomic distance is $d_{Ce-O} = 2.34 \text{ \AA}$. The corresponding Stark energy is $\delta W = \delta P E V$ where $\delta P = \pi n_{Ce-O-Ce}$ is the polarization induced by the valence shift, E is the electric field, and $n_{Ce-O-Ce} = n_{Ce}/2 = 1.3 \cdot 10^{22} \text{ cm}^{-3}$ is the concentration of Ce-O-Ce complexes (as obtained from diffraction data). Such a reorganization of the Ce-O-Ce neighborhood can occur if the characteristic δW will exceed some critical value δW_c . To make a rough estimate of the δW_c let us assume, rather arbitrarily, that the electric field acts similarly to hydrostatic pressure smashing $4f$ Ce core electrons to the delocalized states as described for Ce metal above. This elastic energy can be estimated as the work $\delta W = p \delta V$ produced by $p = 7$ kbar pressure to make a $\delta V/V = 16\%$ volume decrease (experimental data). Equalizing these two energies gives an approximation for the electric switching field

$$E = \frac{p(\delta V/V)}{ed_{Ce-O}n_{Ce}} \sim 1 \text{ MV/cm}, \quad (9)$$

close to the experimentally determined value of about $4 \text{ V}/80 \text{ nm} = 500 \text{ kV/cm}$ shown in Fig. 4.

*Electronic address: rickardb@imit.kth.se

- ¹S. R. Ovshinsky, Phys. Rev. Lett. **36**, 1469 (1968).
- ²B. Fisher, J. Phys. C **8**, 2072 (1975).
- ³W. P. Ballard and R. W. Christy, J. Non-Cryst. Solids **17**, 81 (1975).
- ⁴H. J. Hovel and J. J. Urgell, J. Appl. Phys. **42**, 5076 (1971).
- ⁵H. J. Gao, K. Sohlberg, Z. Q. Xue, H. Y. Chen, S. M. Hou, L. P. Ma, X. W. Fang, S. J. Pang, and S. J. Pennycook, Phys. Rev. Lett. **84**, 1780 (2000).
- ⁶S. Q. Liu, N. J. Wu, and A. Ignatiev, Appl. Phys. Lett. **76**, 2749 (2000).
- ⁷S. Q. Liu, N. J. Wu, and A. Ignatiev, U.S. Patent No. 6 204 139 (20 March 2001).
- ⁸A. Ignatiev, N. J. Wu, S. Q. Liu, and E. J. Charlson, U.S. Patent No. 6 473 332 (29 October 2002).
- ⁹W. W. Zhuang, W. Pan, B. D. Ulrich, J. J. Lee, L. Stecker, A. Burmaster, D. R. Evans, S. T. Hsu, M. Tajiri, A. Shimaoka *et al.*, in *IEDM '02 Digest. International, 8–11 December* (2002), pp. 193–196.
- ¹⁰A. Baikalov, Y. Q. Wang, B. Shen, B. Lorenz, S. Tsui, Y. Y. Sun, Y. Y. Xue, and C. W. Chu, Appl. Phys. Lett. **83**, 957 (2003).
- ¹¹N. A. Tulina, S. A. Zver'kov, A. Arsenov, Y. M. Mukovski, and D. A. Shulyatev, Physica C **385**, 563 (2003).
- ¹²A. Beck, J. G. Bednorz, C. Gerber, C. Rossel, and D. Widmer, Appl. Phys. Lett. **77**, 139 (2000).
- ¹³A. Beck, J. G. Bednorz, C. Gerber, and C. Rossel, WO Patent No. 00/49659 (24 August 2000).
- ¹⁴Y. Watanabe, J. G. Bednorz, A. Bietsch, C. Gerber, D. Widmer, A. Beck, and S. J. Wind, Appl. Phys. Lett. **78**, 3738 (2001).
- ¹⁵C. Rossel, G. I. Meijer, D. Brémaud, and D. Widmer, J. Appl. Phys. **90**, 2892 (2001).
- ¹⁶J. G. Simmons and R. R. Verderber, Proc. R. Soc. London, Ser. A **301**, 77 (1967).
- ¹⁷A. Plecenik, A. Gilabert, K. Frohlich, A. Halabica, M. Pripko, M. G. Medici, J. P. Espinos, and J. P. Holgado, J. Supercond. **15**, 579 (2002).
- ¹⁸M. J. Rozenberg, I. H. Inoue, and M. J. Sanchez, Phys. Rev. Lett. **92**, 178302 (2004).
- ¹⁹L. Tye, N. A. El-Mastry, T. Chikyow, P. McLarty, and S. M. Bedair, Appl. Phys. Lett. **65**, 3081 (1994).
- ²⁰H. B. Lal and V. Pratap, Indian J. Pure Appl. Phys. **16**, 519 (1978).
- ²¹G. Boureau, O. Masoudi, and R. Tetot, Solid State Commun. **79**, 299 (1991).
- ²²W.-C. Tsai and T.-Y. Tseng, J. Mater. Sci.: Mater. Electron. **8**, 313 (1997).
- ²³N. A. Tulina, S. A. Zver'kov, Y. M. Mukovskii, and D. A. Shulyatev, Europhys. Lett. **56**, 836 (2001).
- ²⁴P. Dai, H. Y. Hwang, J. Zhang, J. A. Fernandez-Baca, S.-W. Cheong, C. Kloc, Y. Tomioka, and Y. Tokura, Phys. Rev. B **61**, 9553 (2000).
- ²⁵N. K. Todd, N. D. Mathur, S. P. Isaac, J. E. Evetts, and M. G. Blamire, J. Appl. Phys. **85**, 7263 (1999).
- ²⁶A. Lissauskas, S. I. Khartsev, and A. M. Grishin, Appl. Phys. Lett. **77**, 756 (2000).
- ²⁷J. B. Gunn, Solid State Commun. **1**, 88 (1963).
- ²⁸P. N. Butcher, Rep. Prog. Phys. **30**, 97 (1967).
- ²⁹B. K. Ridley and T. B. Watkins, Proc. Phys. Soc. London **78**, 293 (1961).
- ³⁰N. V. Skorodumova, R. Ahuja, S. I. Simak, I. A. Abrikosov, B. Johansson, and B. I. Lundqvist, Phys. Rev. B **64**, 115108 (2001).
- ³¹S. K. De and S. Chatterje, J. Phys.: Condens. Matter **1**, 1169 (1989).
- ³²S. M. Sze, *Physics of Semiconductor Devices* (Wiley-Interscience, New York, 1981).
- ³³D. D. Koelling, A. M. Boring, and J. H. Wood, Solid State Commun. **47**, 227 (1983).
- ³⁴N. V. Skorodumova, S. I. Simak, B. I. Lundqvist, I. A. Abrikosov, and B. Johansson, Phys. Rev. Lett. **89**, 166601 (2002).
- ³⁵A. W. Lawson and T. Y. Tang, Phys. Rev. **76**, 301 (1949).
- ³⁶A. F. Schuch and J. H. Sturdivant, J. Chem. Phys. **18**, 145 (1950).
- ³⁷B. Coqblin and A. Blandin, Adv. Phys. **17**, 281 (1968).
- ³⁸L. L. Hirst, J. Phys. Chem. Solids **35**, 1285 (1974).